FRIEDRICH-ALEXANDER-UNIVERSITÄT ERLANGEN-NÜRNBERG
INSTITUT FÜR INFORMATIK (MATHEMATISCHE MASCHINEN UND DATENVERARBEITUNG)

Lehrstuhl für Informatik 10 (Systemsimulation)

Lattice Boltzmann simulation of bubbly flows: First results of experimental verification and comparison with Volume of Fluid model

Vivek Buwa, Stefan Donath, Swapna Rabha, Ulrich Rüde

Technical Report 10-4

Lattice Boltzmann simulation of bubbly flows: First results of experimental verification and comparison with Volume of Fluid model

Vivek Buwa[*], Stefan Donath[†], Swapna Rabha[‡], Ulrich Rüde[§]

February 16, 2010

Abstract

Two phase flows appear in nature and in everyday's life. Yet, gas–liquid bubbly flows play also a tremendous role in many engineering applications like loop reactors or metal foaming. Especially for prediction of gas–liquid systems with high gas hold ups an accurate modeling of closure is important. This report presents first results of the validation of a free surface lattice Boltzmann model and a Volume of Fluid method. In a first stage, the rise velocity of single bubbles is examined. Validation occurs by comparing to data of experiments that have been performed. While the overall agreement of the methods to the experimental data is reasonably well, the direct comparison of the methods show deviances that are subject of further studies. The ongoing research work will cover more elaborate single bubble scenarios as well as multiple bubble scenarios.

1 Introduction

Gas–liquid bubbly flows are involved in many engineering applications, for example, in chemical processing, oil and gas industry, biochemical operations etc. Some of the important gas-liquid reactors are bubble columns, stirred tanks and loop reactors. The development of computational flow models, which can be used as a tool for design and scale up of these reactors is of great importance. Over last decade, the hydrodynamics of gas–liquid flows has been investigated by many researchers using the models from computational fluid dynamics (CFD) based on the continuum and the discrete particle approaches. Though, the above mentioned models can predict the time-averaged and dynamic characteristics of gas–liquid quantitatively well for simple systems with low gas hold ups, the quantitative predictions of gas–liquid systems with higher gas hold ups are still out of reach. This is primarily because of the lack of adequate closure models which can account for the effect of bubble shape/size on different forces acting on a bubble and more importantly the influence of neighboring bubbles at high gas volume fractions. It is therefore important to investigate the rise behavior of single and multiple bubbles and to develop accurate closure laws for large-scale CFD models. Many researchers

[*]Department of Chemical Engineering, Indian Institute of Technology Delhi (IIT-Delhi), New Delhi-110 016, India, vvbuwa@chemical.iitd.ac.in

[†]Chair for System Simulation, University of Erlangen-Nuremberg, 91058 Erlangen, Germany, stefan.donath@informatik.uni-erlangen.de

[‡]Department of Chemical Engineering, Indian Institute of Technology Delhi (IIT-Delhi), New Delhi-110 016, India

[§]Chair for System Simulation, University of Erlangen-Nuremberg, 91058 Erlangen, Germany, ulrich.ruede@informatik.uni-erlangen.de

investigated, experimentally [CGW78, KUBE99] and numerically using free surface simulation methods [KUBE99, BT02a, BT02b, SSKS02], the rise behaviour of single and multiple bubbles under different flow conditions and for different liquids; and developed correlations for interphase coupling forces that can account size and shape of bubbles and volume fraction. Some of the important free surface flow simulation methods are Front Tracking (Unverdi and Tryggvason, 1992a, b), Level Set [SSO94, SFSO97], Volume of Fluid [HN81], Lattice Boltzmann method [Suc01, Hän04], etc. In this work, simulations of rise of a single air bubble of different diameter ($0.63 \leq d_B \leq 7.5$mm) in water were performed using both the lattice Boltzmann method and the Volume of Fluid and predictions were compared with the experimental data.

2 Description of Methods

In this report, the volume of fluid (VoF) method developed and lattice Boltzmann method (LBM) was used to simulate the rise behavior of single bubbles. This section gives a short overview of the two models.

2.1 Volume of Fluids

In this method, a particular phase q is identified by its volume fraction (α_q) in a computational cell as follows:

if $\alpha_q = 1$; cell is full of qth (secondary) phase
if $\alpha_q = 0$; cell is full of pth (primary) phase
if $0 < \alpha_q < 1$; cell contains the interface between the pth and qth phases.

A single set of Navier-Strokes equation for an incompressible Newtonian flow was solved as,

$$\frac{\partial}{\partial t}(\rho\vec{v}) + \nabla\cdot(\rho\vec{v}\vec{v}) = -\nabla p + \nabla\cdot\left[\mu\left(\nabla\vec{v} + (\nabla\vec{v})^T\right)\right] + \rho\vec{g} + \vec{F}\,, \tag{1}$$

where $\vec{v}$ is the velocity vector and $\vec{F}$ is the surface force per unit volume. When a control volume is not entirely occupied by one phase, mixture properties (estimated by Equations 2 and 3) were used to solve the Equation 1:

$$\rho = \alpha_q\rho_q + (1-\alpha_q)\rho_p\,, \tag{2}$$

$$\mu = \alpha_q\mu_q + (1-\alpha_q)\mu_p\,. \tag{3}$$

The CSF model of Brackbill et al. [BKZ92] was used to compute the surface tension force as a source term in the momentum equation for the cells containing the interface. The expression for $\vec{F}$ is given by

$$\vec{F} = \sigma\frac{\rho\kappa\vec{n}}{\frac{1}{2}(\rho_p+\rho_q)}\,, \tag{4}$$

where σ is the coefficient of surface tension, $\hat{n}$ is the surface normal which is proportional to the gradient of volume fraction, κ is the local surface curvature calculated as $\kappa = -(\nabla\cdot\hat{n})$, where $\hat{n} = \vec{n}/|\vec{n}|$ and $\vec{n} = \nabla\alpha_q$. The geometric reconstruction scheme [You82] based on piecewise linear approach [RK98] was used for the reconstruction of the interface. In the VOF approach, the reconstructed interface is advected by solving an advection equation for the volume fraction of the secondary phase. or the qth phase, advection equation is written as

$$\frac{\partial}{\partial t}(\alpha_q\rho_q) + \nabla\cdot(\alpha_q\rho_q\vec{v}_q) = 0\,. \tag{5}$$

The primary phase volume fraction is computed from the equation

$$\alpha_p + \alpha_q = 1\,. \tag{6}$$

Equations 1 and 5 were solved using the commercial flow solver Fluent 6.2

2.2 LBM Free Surface

The lattice Boltzmann method is based on lattice gas cellular automata, and can be used to compute time-dependent fluid flows. It has been shown that the LBM can be directly derived from the continuous Boltzmann equation [HL97]. It is equivalent to an explicit finite difference scheme of the Navier-Stokes equations with second order accuracy in space and first order in time [JKL05].

The free surface extension introduces different types of lattice sites (*cells*), representing regions of liquid, gas, or of the interface in between, respectively. To simplify the method, gas flow is neglected and thus, in gas cells no computation takes place. Influence of the gas is only modeled by its gas pressure and the forces resulting from surface tension. While in liquid cells a standard single phase LBM, as described in the first part of this section, is performed, for interface cells special boundary conditions, which are outlined in the second part of this section, introduce the forces exerted by the gas phase.

2.2.1 Single Phase Lattice Boltzmann Method

This implementation of LBM uses the so-called LBGK [MZ88] model which is most common. In tensor notation, the time and space discretization of this model is given by

$$f_\alpha(\vec{x}+\vec{e}_\alpha\delta t, t+\delta t) - f_\alpha(\vec{x},t) = -\frac{\delta t}{\tau}\left[f_\alpha(\vec{x},t) - f_\alpha^{(eq)}(\rho(\vec{x},t),\vec{u}(\vec{x},t))\right], \tag{7}$$

where $f_\alpha(\vec{x},t)$ is the discrete particle distribution function (PDF) which is defined as the expected fraction of particles in the volume δx^3 located at the lattice position $\vec{x}$ with the lattice velocity $\vec{e}_\alpha$. For the sake of simplicity, quantities depending on $\vec{x}$ and t will be written without their dependencies, e.g. $f_\alpha = f_\alpha(\vec{x},t)$. The D3Q19 model [MSYL00], illustrated in Figure 1, uses $\alpha \in [0,18]$ lattice directions in three dimensions. For the isothermal case, the equilibrium distribution

$$f_\alpha^{(eq)}(\rho,\vec{u}) = \rho\cdot w_\alpha \cdot \left[1 + \frac{1}{c_s^2}(\vec{e}_\alpha\cdot\vec{u}) + \frac{1}{2c_s^4}(\vec{e}_\alpha\cdot\vec{u})^2 - \frac{1}{2c_s^2}\vec{u}^2\right] \tag{8}$$

depends on the macroscopic velocity $\vec{u}$ (Equation 9) and the macroscopic density ρ (Equation 10). It is a Maxwell-Boltzmann distribution function discretized for low mach numbers. In the D3Q19 model $c_s = \frac{1}{\sqrt{3}}$, which is the thermodynamic speed of sound. Additionally, it has the same order of magnitude as the quadratic mean of the fluid particles' molecular velocities. The macroscopic quantities of interest $(\rho,\vec{u})$ can be determined from the first two moments of the distribution functions:

$$\rho\vec{u} = \sum_{\alpha=0}^{18}\vec{e}_\alpha\cdot f_\alpha = \sum_{\alpha=0}^{18}\vec{e}_\alpha\cdot f_\alpha^{(eq)}(\rho,\vec{u}), \tag{9}$$

$$\rho = \sum_{\alpha=0}^{18} f_\alpha \qquad = \sum_{\alpha=0}^{18} f_\alpha^{(eq)}(\rho,\vec{u}). \tag{10}$$

For the LBM, the macroscopic pressure is given by $p = c_s^2\rho$. The lattice velocities $\vec{e}_\alpha$ and the lattice weights w_α for the D3Q19 model are:

$$\vec{e}_\alpha = \begin{cases} (0,0,0), \\ (\pm1,0,0),(0,\pm1,0),(0,0,\pm1), \\ (\pm1,\pm1,0),(0,\pm1,\pm1),(\pm1,0,\pm1) \end{cases} \qquad w_\alpha = \begin{cases} 1/3, & \alpha = \text{C} \\ 1/18, & \alpha = \text{W, E, N, S, T, B} \\ 1/36, & \alpha = \text{NW, NE, SW, SE, TN, TS,} \\ & \quad\ \text{BN, BS, TW, TE, BW, BE} \end{cases}$$

For a detailed description of the LBM see [Hän04, YMLS03, HL97].

2.2.2 Free Surface Extension

The free surface extension mainly consists of a special boundary treatment in interface cells, which are also used to explicitly track the surface and mass. Similar to VoF, an additional variable, the fill value φ, specifies the portion of the cell's volume filled with liquid. By definition, φ is 1 for liquid cells and 0 for gas cells. Thus, the mass contained in an interface cell is

$$m = \varphi\,\delta x^3\cdot\rho. \tag{11}$$

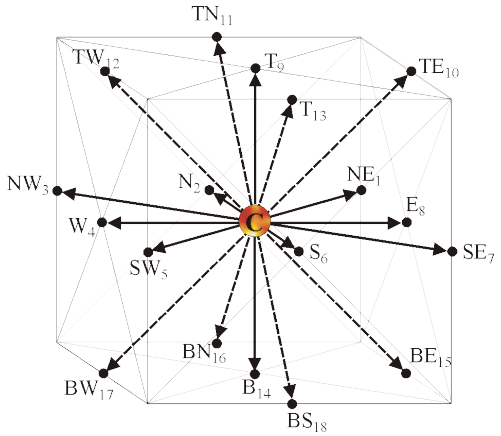

Figure 1: Discretization model D3Q19 in three dimensions with 18 discrete velocity directions and the center representing the fraction of non-moving particles.

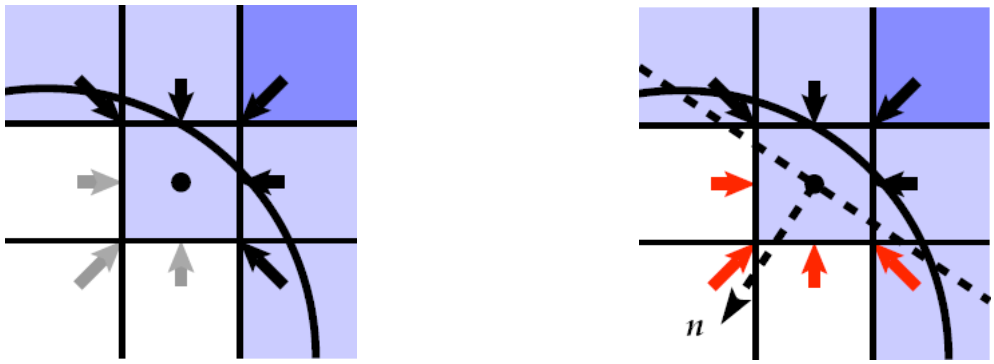

Figure 2: Instead of reconstructing only the undefined distribution functions from gas phase in an interface cell (gray arrows in left image), the set of distribution functions pointing anti-parallel to surface normal $\vec{n}$ ($\vec{e}_\alpha \cdot \vec{n} < 0$, colored arrows in right image) are reconstructed [Poh08].

While mass transfer for liquid cells is modeled by the streaming of distribution functions as described in the previous part of this section, for interface cells mass exchange is explicitly modeled as

$$\Delta m = \begin{cases} 0 & \text{if } (\vec{x} + \vec{e}_\alpha) \text{ is gas,} \\ f_{\bar{\alpha}}(\vec{x} + \vec{e}_\alpha, t) - f_\alpha(\vec{x}, t) & \text{if } (\vec{x} + \vec{e}_\alpha) \text{ is liquid,} \\ \frac{1}{2}\left[\varphi(\vec{x}, t) + \varphi(\vec{x} + \vec{e}_\alpha, t)\right]\left[f_{\bar{\alpha}}(\vec{x} + \vec{e}_\alpha, t) - f_\alpha(\vec{x}, t)\right] & \text{if } (\vec{x} + \vec{e}_\alpha) \text{ is interface,} \end{cases}$$

where $\bar{\alpha}$ denotes the opposite direction of α. Accordingly, the transferred mass equals the difference of the particle distributions exchanged by two neighboring cells, because their volumes are the same. As a consequence, for mass exchange between two interface cells, the distributions have to be weighted by the fluid volumes.

Since no gas flow is simulated, there are no valid PDFs in gas cells. Hence, the stream step cannot be performed directly, which is the reason for the introduction of interface cells. In the interface cells, the PDFs that are missing from the gas phase are reconstructed such that the collision can take plase as usual. The missing PDFs are computed such that the force performed by the liquid balances those arising from the gas pressure and surface tension, and the velocities of liquid and gas are equal. Both requirements are met by the reconstruction method proposed by Körner et al. [KTH+05], where all PDFs with $\vec{e}_\alpha \cdot \vec{n} < 0$ are calculated like

$$f_\alpha(\vec{x} - \vec{e}_\alpha \delta t, t + \delta t) = f_\alpha^{eq}(\rho_G, \vec{u}) + f_{\bar{\alpha}}^{eq}(\rho_G, \vec{u}) - f_{\bar{\alpha}}(\vec{x}, t)\,. \tag{12}$$

The gas density ρ_G is influenced by the gas pressure p_G, the surface tension σ as well as curvature κ, and is calculated by

$$\rho_G = \frac{1}{c_s^2}\left(p_G + 2\sigma\kappa(\vec{x},t)\right) . \tag{13}$$

The second term arises from the energy balance $p_G \cdot dV = \sigma \cdot dA$ equalling the surface tension on the surface dA to the gas pressure in volume dV. The gas pressure is equal at any point inside the bubble and can be calculated from its volume: Each bubble is characterized by its initial volume V^{init} and its current volume $V(t)$. Hence, the normalized gas pressure is calculated as

$$p_G = \frac{V^{init}}{V(t)} . \tag{14}$$

In terms of computational effort, the most complex part of this method is determination of the curvature κ in each time step. For this, the surface normal $\vec{n}$ is computed as the gradient of the fill values using a Parker-Youngs approximation [PY92]. With the normal and fill value, surface points are determined for each cell, which serve as input for computation of curvature κ. More details on this algorithm can be found in [Poh08].

3 Valid Parameter Range of LBM simulation

For the definition of proper test cases, a study for valid parameter ranges, the free surface LBM can handle, had to be carried out. Due to restrictions that come from numerics and the derivation of the method, limits in the lattice parameter space have to be translated to physical dimensions in order to assess the feasibility of proper scenarios. Most limits can be met by choosing an appropriate spatial resolution. However, a finer spatial resolution results in the need for a larger amount of memory. Thus, as long as the method remains in the continuum range, the available memory dictates the possible simulation scenarios.

This section specifies the maximum bubble sizes for a single rising bubble scenario as well as the maximum number of rising bubbles, depending on the liquid properties viscosity, density and surface tension. In the derivation of the LBM, several assumptions have to be made that lead to the need of a viscosity correction, which in term limits the valid range for the relaxation factor to

$$0.5 \geq \frac{1}{\tau} \leq 2.0 . \tag{15}$$

However, disturbing effects from the discretization scheme, boundary conditions, and others further constrict this range. From simulation experiments we know, that simulations generally remain stable, if

$$\frac{1}{\tau} \leq 1.96 . \tag{16}$$

Thus, for calculation of the ultimate limits, in the following a value of $1/\tau = 1.9599$ is assumed. Furthermore, from numerical experiments a maximal value for the lattice surface tension of $\sigma^* = 0.055$ could be derived. Beyond this value numerical instabilities due to too high forces can arise throughout the simulation.

For a rising bubble, the most important dimensionless numbers are the Reynolds (Re), Morton (Mo), and the Eötvös (Eo) number:

$$Re = \frac{U_T d_B \rho}{\mu} , \tag{17}$$

$$Mo = \frac{g\mu^4 \Delta\rho d_B^2}{\rho^2\sigma^3} , \tag{18}$$

$$Eo = \frac{g\Delta\rho d_B^2}{\sigma} , \tag{19}$$

where U_T is the rising velocity of the bubble, d_B is the diameter of a sphere with the same volume as the bubble, ρ is the density and μ the dynamic viscosity of the liquid phase, g is the gravitational acceleration, σ describes the surface tension between the liquid and gas phase, and $\Delta\rho$ is the density

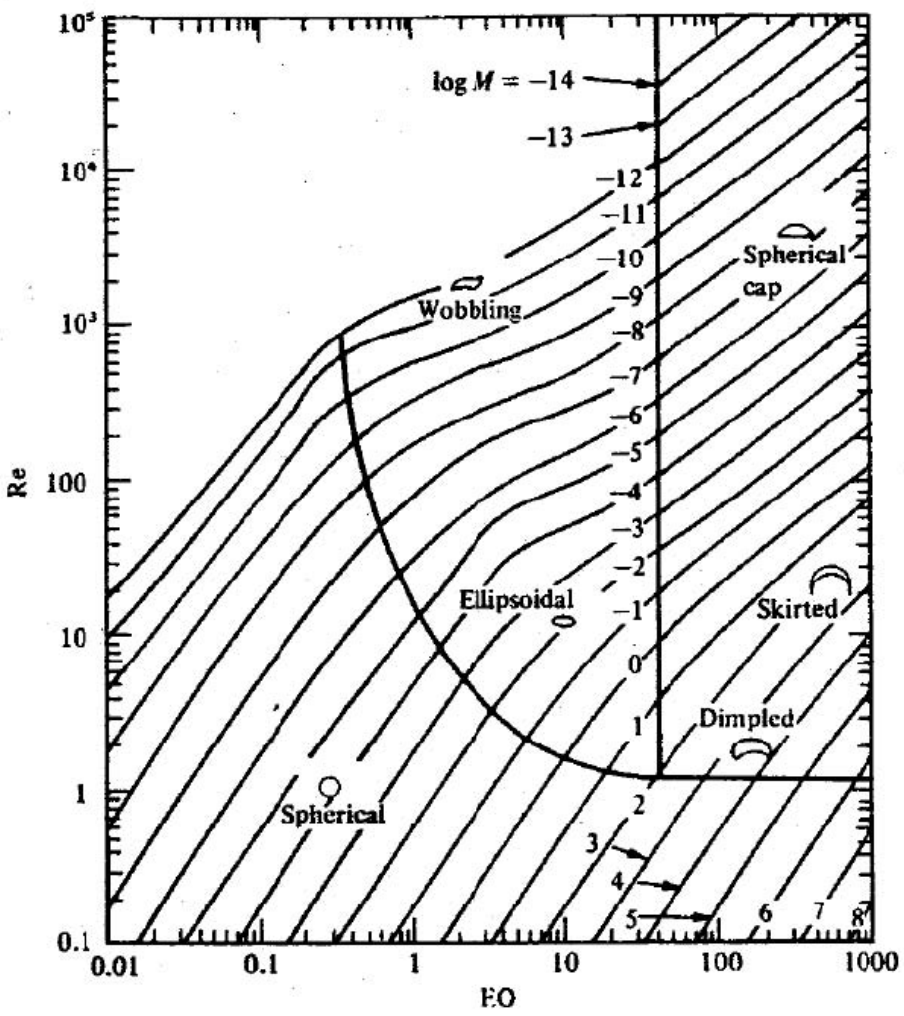

Figure 3: Shapes of a rising bubble depending on the Reynold-, Eötvös-, and Morton-number [Töl01].

difference of the liquid phase and the bubble. Depending on these numbers, it is possible to characterize the regime and thus the shape of the bubble as depicted in Figure 3.

With the aforementioned restrictions and the characteristic quantities of the observed fluid, a maximal lattice spacing δx and can be derived from the kinematic viscosity ν, the liquid's density ρ, and surface tension σ by

$$\delta x = \frac{\rho\,\sigma^*\nu^2}{\sigma\nu^{*2}}\,, \tag{20}$$

with

$$\nu^* = \frac{1}{c_s^2}\left(\tau - \frac{\delta t^*}{2}\right)\,, \tag{21}$$

where $\delta t^* = 1$ and $\sigma^* = 0.055$. Equation 20 can be derived from the parametrization for ν and σ. From δx, the temporal spacing δt is computed via the parametrization of ν. The lattice diameter of the bubble is $d_B^* = \frac{d_B}{\delta x}$.

In order to evaluate the maximal possible simulation scenarios, the memory consumption has to be estimated. In the waLBerla implementation, the free surface extension consumes about 550 Bytes per lattice site. Studying the rise velocity of a single rising bubble in a tube with noslip boundaries, the boundaries have to be apart far enough to reduce their influence on the bubble movement. An overall domain width of five bubble diameters has been proved to be sufficient. To cover a considerable long movement, the domain's height should be at least $17.5\,d_B$. Thus, the overall memory consumption M_{rb} of the rising bubble scenario sums up to

$$M_{\mathrm{rb}} = \lceil 5\,d_B^* \rceil^2 \cdot \lceil 17.5\,d_B^* \rceil \cdot 550\,\mathrm{Bytes}\,. \tag{22}$$

Another scenario simulates several rising bubbles set up in a cubic arrangement, each of the bubbles in a distance of one bubble diameter from the other, in a domain with periodic boundary conditions. Assuming thus, that an edge of the domain is a multiple of the doubled bubble diameter, the maximum number of bubbles N_B that can be simulated on a computer like the HLRB 2 [HLR], featuring 40 TBs of memory, can be estimated with

$$N_B = \left\lfloor \frac{\left\lfloor \sqrt[3]{\frac{40\,\mathrm{TBs}}{550\,\mathrm{Bytes}}} \right\rfloor}{\lceil 2\,d_B^* \rceil} \right\rfloor^3 = \left\lfloor \frac{4308}{\lceil 2\,d_B^* \rceil} \right\rfloor^3 . \tag{23}$$

Table 1 lists physical and lattice quantities of an air-water system, the dimensionless numbers, as well as M_{rb} and N_B for different bubble diameters. Note that the columns for 10 mm and 20 mm bubbles show theoretical values only. Bubbles of this size in an air-water system would break up, which is not handled by the simulation code yet. In order to demonstrate the feasible fluid systems, the Tables 2 to 4 show the same corresponding values for systems altered in the fluid's surface tension, viscosity, and density, respectively. Accordingly, even for a fluid with doubled surface tension (Table 2 with system *air-model fluid II*) an ensemble of multiple bubbles can be simulated up to bubble diameters of 20 mm. However, the single rising bubble scenario is not achievable due to its memory requirement of 50 TB. Obviously, fluids with smaller surface tension can be easily handled. Table 3 shows that more viscous fluids lie well below the critical values and thus represent no challenge for the solver. Doubling the density leads to the same resource requirements of the simulation like the doubled surface tension (compare *air-model fluid IV* in Table 4 with *air-model fluid II* in Table 2). Again, lower densities lie below the boundary induced by the maximum lattice surface tension.

4 Validation and Comparison

The experimental investigations of rise of single air bubble in water were carried out by injecting air bubbles through stainless steel needles in a glass column (height, $H = 600$mm; width, $W = 150$mm; depth, $D = 150$mm) filled with water (de-mineralized) as shown in Figure 4. A high-speed digital camera (Fastec imaging, USA) capable of capturing 1000 fps was used to record bubble trajectories. The average (sphere-equivalent) bubble diameters considered in the experiments were $d_B = 0.635(\pm 0.005)$, $3.0(\pm 0.1)$, $4.85(\pm 0.1)$, and $7.5(\pm 0.1)$mm. The average (sphere-equivalent) bubble diameter was calculated by taking an average over 20 bubbles (just after their detachment from the needles). The

Table 1: Dimensionless numbers, memory consumption and maximum number of bubbles for an *air-water* system.

Fluid properties

Property		Value	Unit
dynamic viscosity	μ	$1{\cdot}10^{-3}$	$\frac{Ns}{m^2}$
kinematic viscosity	ν	$1{\cdot}10^{-6}$	$\frac{m^2}{s}$
liquid density	ρ	$1{\cdot}10^{3}$	$\frac{kg}{m^3}$
surface tension	σ	$7.2{\cdot}10^{-2}$	$\frac{N}{m}$

Discretization

Property		Value	Unit
lattice width	δx	$6.57{\cdot}10^{-5}$	m
time step	δt	$1.47{\cdot}10^{-5}$	s
lattice viscosity	ν^*	$3.41{\cdot}10^{-3}$	
lattice surface tension	σ^*	$5.50{\cdot}10^{-2}$	

Bubble sizes					
d_B	1 mm	3 mm	8 mm	10 mm	20 mm
d_B^*	15.22	45.67	121.78	152.23	304.45
Dimensionless numbers					
Re	200	600	1600	2000	4000
Mo	$2.63 \cdot 10^{-11}$	$2.63 \cdot 10^{-11}$	$2.63 \cdot 10^{-11}$	$2.63 \cdot 10^{-11}$	$2.63 \cdot 10^{-11}$
Eo	0.14	1.23	8.72	13.63	54.5
Single bubble scenario					
Domain size	$77^2 \cdot 267$	$229^2 \cdot 800$	$609^2 \cdot 2132$	$762^2 \cdot 2664$	$1523^2 \cdot 5328$
	$1.58 \cdot 10^6$	$4.2 \cdot 10^7$	$7.9 \cdot 10^8$	$1.55 \cdot 10^9$	$1.24 \cdot 10^{10}$
Memory M_{rb}	811 MB	21.5 GB	99 GB	405 GB	6.3 TB
Multiple bubbles scenario					
Number of bubbles N_B	138^3	46^3	17^3	14^3	7^3
	$2.6 \cdot 10^6$	97336	4913	2744	343

Table 2: Dimensionless numbers, memory consumption and maximum number of bubbles for a system similar to air-water, except for the doubled surface tension (*air-model fluid II*).

Fluid properties

Property		Value	Unit
dynamic viscosity	μ	$1{\cdot}10^{-3}$	$\frac{Ns}{m^2}$
kinematic viscosity	ν	$1{\cdot}10^{-6}$	$\frac{m^2}{s}$
liquid density	ρ	$1{\cdot}10^{3}$	$\frac{kg}{m^3}$
surface tension	σ	$1.4{\cdot}10^{-1}$	$\frac{N}{m}$

Discretization

Property		Value	Unit
lattice width	δx	$3.28{\cdot}10^{-5}$	m
time step	δt	$3.68{\cdot}10^{-6}$	s
lattice viscosity	ν^*	$3.41{\cdot}10^{-3}$	
lattice surface tension	σ^*	$5.50{\cdot}10^{-2}$	

Bubble sizes					
d_B	1 mm	3 mm	8 mm	10 mm	20 mm
d_B^*	30.45	91.34	243.56	304.45	608.90
Dimensionless numbers					
Re	200	600	1600	2000	4000
Mo	$3.29 \cdot 10^{-12}$	$3.29 \cdot 10^{-12}$	$3.29 \cdot 10^{-12}$	$3.29 \cdot 10^{-12}$	$3.29 \cdot 10^{-12}$
Eo	$6.8 \cdot 10^{-2}$	0.61	4.36	6.81	27.25
Single bubble scenario					
Domain size	$153^2 \cdot 533$	$457^2 \cdot 1599$	$1218^2 \cdot 4263$	$1523^2 \cdot 5328$	$3045^2 \cdot 10656$
	$1.25 \cdot 10^7$	$3.3 \cdot 10^8$	$6.3 \cdot 10^9$	$1.24 \cdot 10^{10}$	$9.88 \cdot 10^{10}$
Memory M_{rb}	6.39 TB	171.1 GB	3.2 TB	6.3 TB	50.6 TB
Multiple bubbles scenario					
Number of bubbles N_B	70^3	23^3	8^3	7^3	3^3
	$3.43 \cdot 10^5$	12167	512	343	27

Table 3: Dimensionless numbers, memory consumption and maximum number of bubbles for a system similar to air-water, except for the higher viscosity (*air-model fluid III*).

Fluid properties

Property		Value	Unit
dynamic viscosity	μ	$5{\cdot}10^{-2}$	$\frac{Ns}{m^2}$
kinematic viscosity	ν	$5{\cdot}10^{-5}$	$\frac{m^2}{s}$
liquid density	ρ	$1{\cdot}10^{3}$	$\frac{kg}{m^3}$
surface tension	σ	$7.2{\cdot}10^{-2}$	$\frac{N}{m}$

Discretization

Property		Value	Unit
lattice width	δx	$3.41{\cdot}10^{-3}$	m
time step	δt	$1.64{\cdot}10^{-1}$	s
lattice viscosity	ν^*	1.84	
lattice surface tension	σ^*	$5.50{\cdot}10^{-2}$	

Bubble sizes

d_B	1 mm	3 mm	8 mm	10 mm	20 mm
d_B^*	$6 \cdot 10^{-3}$	$2 \cdot 10^{-2}$	$5 \cdot 10^{-2}$	$6 \cdot 10^{-2}$	0.12

Dimensionless numbers

Re	4	12	32	40	80
Mo	$1.64 \cdot 10^{-4}$	$1.64 \cdot 10^{-4}$	$1.64 \cdot 10^{-4}$	$1.64 \cdot 10^{-4}$	$1.64 \cdot 10^{-4}$
Eo	0.14	1.23	8.72	13.63	54.5

Simulation scenarios

Not limited by lattice surface tension (sufficient cells for accurate curvature calculation).

Table 4: Dimensionless numbers, memory consumption and maximum number of bubbles for a system similar to air-water, except for the higher density (*air-model fluid IV*).

Fluid properties

Property		Value	Unit
dynamic viscosity	μ	$1{\cdot}10^{-3}$	$\frac{Ns}{m^2}$
kinematic viscosity	ν	$5{\cdot}10^{-7}$	$\frac{m^2}{s}$
liquid density	ρ	$2{\cdot}10^{3}$	$\frac{kg}{m^3}$
surface tension	σ	$7.2{\cdot}10^{-2}$	$\frac{N}{m}$

Discretization

Property		Value	Unit
lattice width	δx	$3.28{\cdot}10^{-5}$	m
time step	δt	$7.36{\cdot}10^{-6}$	s
lattice viscosity	ν^*	$3.41{\cdot}10^{-3}$	
lattice surface tension	σ^*	$5.50{\cdot}10^{-2}$	

Bubble sizes

d_B	1 mm	3 mm	8 mm	10 mm	20 mm
d_B^*	30.45	91.34	243.56	304.45	608.90

Dimensionless numbers

Re	400	1200	3200	4000	4000
Mo	$1.31 \cdot 10^{-11}$	$1.31 \cdot 10^{-11}$	$1.31 \cdot 10^{-11}$	$1.31 \cdot 10^{-11}$	$3.29 \cdot 10^{-12}$
Eo	0.27	2.45	17.44	27.25	109

Simulation scenarios

Simulation scenarios similar to Table 2.

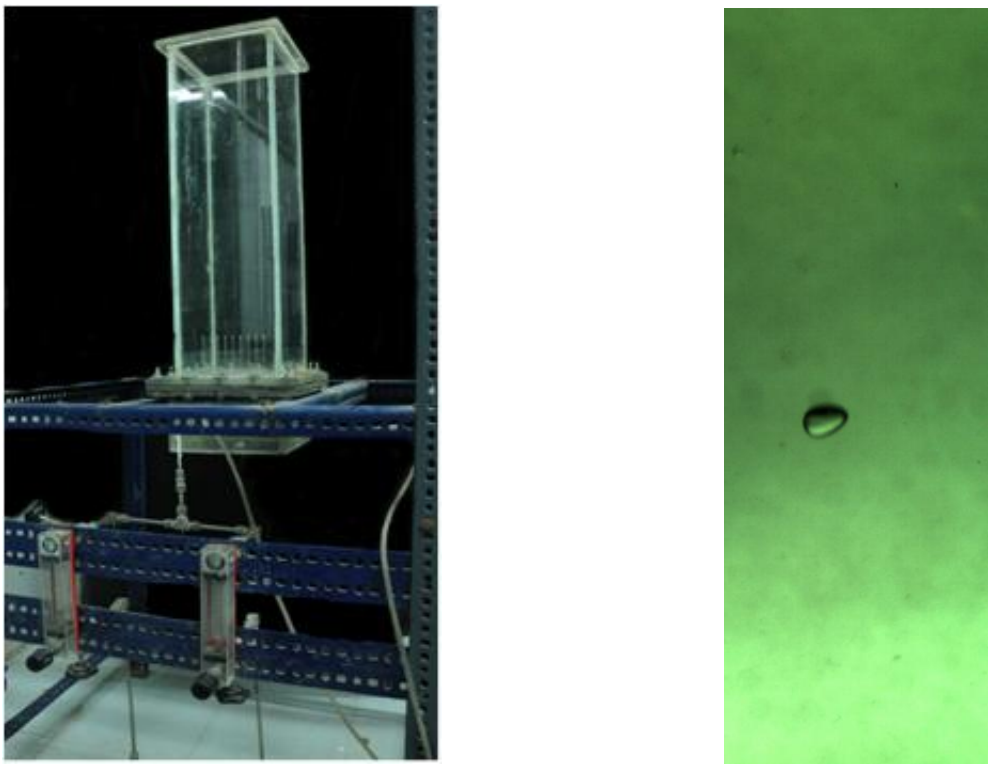

Figure 4: Experimental setup and snapshot of rise of single isolated bubble ($d_B = 4.85$mm).

measured rise velocities of single isolated bubbles of different sizes ($0.635 \leq d_B \leq 7.5$mm) were compared with the measurement of Clift et al. [CGW78] to benchmark our measurements. A snapshot of rise of single isolated bubble ($d_B = 4.85$mm) is shown in Figure 4.

The comparison of simulated rise velocities (using VoF and LBM method) with the measurements for air bubbles with $d_B = 0.635$, 3.0 and 7.5 mm is shown in Figure 5. The time scale in the figure begins at 0.04s because the starting behavior of the bubble differs too much between simulation and experiment. This is due to the different initial setups: In the experiment the gas phase has not a spherical shape and already starts with a certain velocity at the inlet, while the simulation starts with a perfect sphere in rest.

The VoF predictions agree reasonably well with the measurements for $d_B = 7.5$mm. The agreement is not so good for $d_B = 3$mm, and there are difficulties in predicting the rise of bubbles with $d_B = 0.635$mm. The primary reason is that a much finer grid has to be used to resolve the smaller bubbles adequately. Thus, ongoing work concerns implementation of refined grid simulations.

In contrast, LBM simulations predict well the two smaller bubbles with $d_B = 0.635$mm and $d_B = 3$mm. For a well-conditioned simulation of a bubble with $d_b = 7.5$mm the required resolution demands for large system sizes which make runs with tousands of processors necessary. Due to technical problems this could not be achieved up to now.

Due to the large deviations in the experimental results a relative error of the simulations' accuracy is hard to define. It is known that impurities in the water influence the bubble rise velocities. Unfortunately, it is difficult to capture these effects in simulations. Considering this, it is save to argue that both numerical methods are reasonably well within the confidence intervals of the experimental data. The discrepancy between the two methods (as can bee seen for the case of $d_B = 3$mm) has to be further examined. Most likely the reason is the strong sensitivity of the LBM to the lattice viscosity in the extreme regions of the range of value of the relaxation factor $\frac{1}{\tau}$. Only small variations can result in errors which may have an effect on rise velocity.

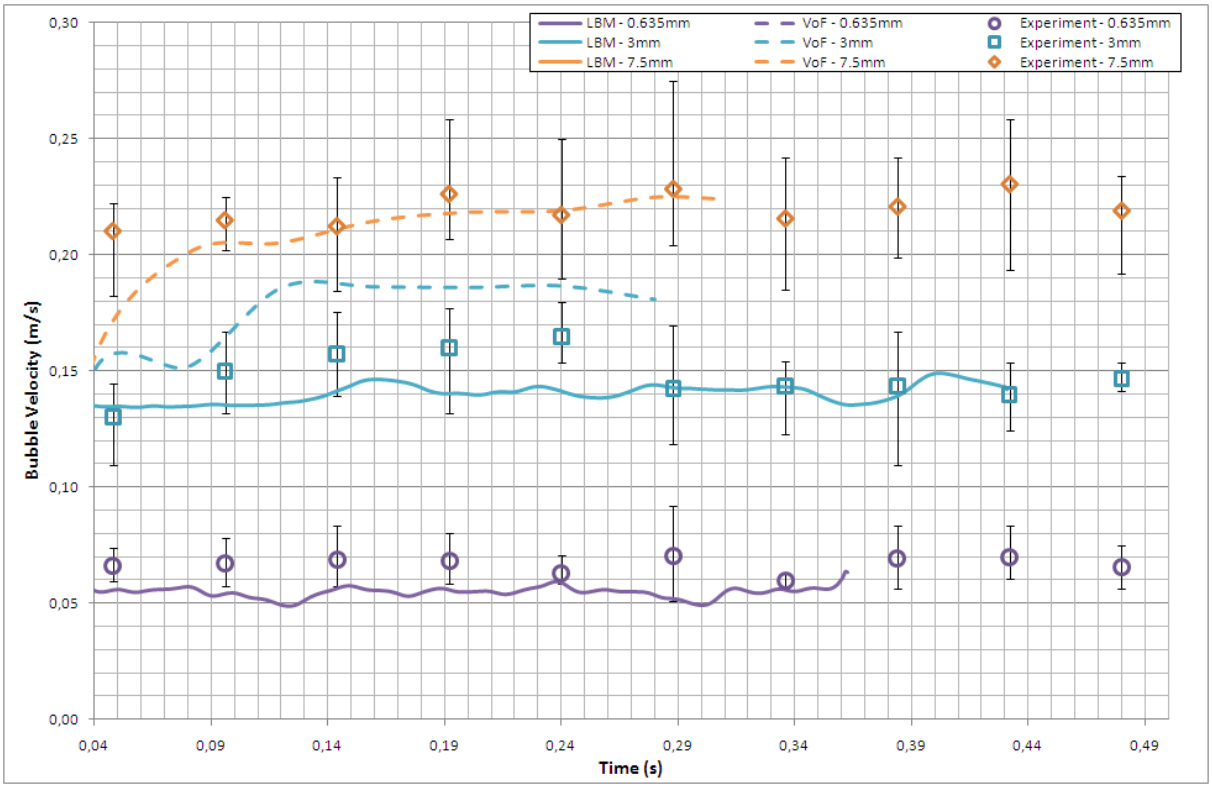

Figure 5: Comparison of experiments with LBM and VoF simulations.

5 Conclusion

An interesting field of research is the predicition of gas–liquid systems with high gas hold ups. For an accurate simulation, the model has to take the effect of bubble shape and size on different forces acting on a bubble into account. The aim of this work is to experimentally verify and compare a free surface lattice Boltzmann method and a Volume of Fluid method. Whereas first scenarios cover the rise of single bubbles of different size, later on scenarios with multiple bubbles are planned. In this report, the current status of the validation of single bubble simulations is presented. The results show that the methods can coincide well with the experimental measurements. However, the experiments show large deviations for different runs and thus it is not possible to quantify the error of the simulations exactly. Moreover, the methods have been found to differ in their predictions which is attributed to numerical sensitivity of the lattice viscosity in the lattice Boltzmann method.
The next steps of this work concern investigation in finer or refined grids in order to make simulation of small bubbles with Volume and Fluid and large bubbles with lattice Boltzmann possible. With these results, future work may deal with multiple bubble scenarios.

References

[BKZ92] J.U. Brackbill, D.B. Kothe, and C. Zemach, *A continuum method for modeling surface tension*, Journal of Computational Physics **100** (1992), 335.

[BT02a] B. Bunner and G. Tryggvason, *Dynamics of homogeneous bubbly flows: Part 1: Rise velocity and microstructure of the bubbles*, Journal of Fluid Mechanics **466** (2002), 17–52.

[BT02b] ———, *Dynamics of homogeneous bubbly flows: Part 2: fluctuations of the bubbles and the liquid*, Journal of Fluid Mechanics **466** (2002), 53–85.

[CGW78] R. Clift, J.R. Grace, and M.E. Weber, *Bubbles, drops and particles*, Academic Press, 1978.

[Hän04] D. Hänel, *Molekulare Gasdynamik*, Springer, 2004.

[HL97] X. He and L.-S. Luo, *Theory of the lattice Boltzmann method: From the Boltzmann equation to the lattice Boltzmann equation*, Phys. Rev. E **56** (1997), no. 6, 6811–6817.

[HLR] HLRB2, *http://www.lrz-muenchen.de/services/compute/hlrb/*.

[HN81] C. W. Hirt and B. D. Nichols, *Volume of fluid /vof/ method for the dynamics of free boundaries*, Journal of Computational Physics **39** (1981), 201–225.

[JKL05] M. Junk, A. Klar, and L.-S. Luo, *Asymptotic analysis of the lattice Boltzmann equation*, J. Comp. Phys. **210** (2005), no. 2, 676–704.

[KTH+05] Carolin Körner, Michael Thies, Torsten Hofmann, Nils Thürey, and Ulrich Rüde, *Lattice Boltzmann model for free surface flow for modeling foaming*, J. Stat. Phys. **121** (2005), no. 1–2, 179–196.

[KUBE99] R. Krishna, M.I. Urseanu, J.M. Van Baten, and J. Ellenberger, *Rise velocity of a swarm of large gas bubbles in liquids*, Chemical Engineering Science **54** (1999), 171–183.

[MSYL00] R. Mei, W. Shyy, D. Yu, and L.-S. Luo, *Lattice Boltzmann Method for 3-D Flows with Curved Boundary*, J. Comp. Phys. **161** (2000), 680 – 699.

[MZ88] G. McNamara and G. Zanetti, *Use of the boltzman equation to simulate lattice gas automata*, Phys. Rev. Lett. **61** (1988), 2332 – 2335.

[Poh08] Thomas Pohl, *High Performance Simulation of Free Surface Flows Using the Lattice Boltzmann Method*, Ph.D. thesis, Univ. of Erlangen, 2008.

[PY92] B. J. Parker and D. L. Youngs, *Two and three dimensional Eulerian simulation of fluid flow with material interfaces*, Tech. Report 01/92, UK Atomic Weapons Establishment, Berkshire, 1992.

[RK98] William J. Rider and Douglas B. Kothe, *Reconstructing volume tracking,*, Journal of Computational Physics **141** (1998), no. 2, 112–152.

[SFSO97] Mark Sussman, Emad Fatemi, Peter Smereka, and Stanley Osher, *An improved level set method for incompressible two-phase flows*, Computers and Fluids **27** (1997), 663–680.

[SSKS02] K. Sankaranarayanan, X. Shan, I.G. Kevrekidis, and S. Sundaresan, *Analysis of drag and virtual mass forces in bubbly suspensions using an implicit formulation of the lattice Boltzmann method*, Journal of Fluid Mechanics **452** (2002), 61–96.

[SSO94] Mark Sussman, Peter Smereka, and Stanley Osher, *A level set approach for computing solutions to incompressible two-phase flow*, J. Comput. Phys. **114** (1994), no. 1, 146–159.

[Suc01] S. Succi, *The lattice Boltzmann equation for fluid dynamics and beyond*, Oxford University Press, 2001.

[Töl01] Jonas Tölke, *Gitter-Boltzmann-Verfahren zur Simulation von Zweiphasenströmungen*, Ph.D. thesis, Technical University of Munich, 2001.

[YMLS03] D. Yu, R. Mei, L.-S. Luo, and W. Shyy, *Viscous flow computation with method of lattice Boltzmann equation*, Prog. Aero. Sci. **39** (2003), 329 – 367.

[You82] D.L. Youngs, *Time-dependent mutli-material flow with large fluid distortion*, Numerical Methods for Fluid Dynamics (K. Morton and M. Baines, eds.), Academic Press, 1982, pp. 273–285.